

# Light by Light Scattering at High Energy: a Tool to Reveal New Particles <sup>†</sup>

G.J. Gounaris<sup>a</sup>, P.I. Porfyriadis<sup>a</sup> and F.M. Renard<sup>b</sup>

<sup>a</sup>Department of Theoretical Physics, University of Thessaloniki,  
Gr-54006, Thessaloniki, Greece.

<sup>b</sup>Physique Mathématique et Théorique, UMR 5825  
Université Montpellier II, F-34095 Montpellier Cedex 5.

## Abstract

We point out a few remarkable properties of the  $\gamma\gamma \rightarrow \gamma\gamma$  process at high energy, which should allow to search for effects of new particles and interactions. We give illustrations with threshold effects due to pairs of new charged particles (charginos, charged Higgs particles, sfermions), resonance effects due to  $s$ -channel production of neutral scalars (standard or supersymmetric neutral Higgs particles or technipions) and unitarity saturating amplitudes due to a strongly interacting sector. The use of polarized photon beams is also briefly discussed.

---

<sup>†</sup>Partially supported by the NATO grant CRG 971470 and by the Greek Government grant PENED/95 K.A. 1795.

In this letter we point out a few striking properties of the  $\gamma\gamma \rightarrow \gamma\gamma$  scattering amplitude at high energy, which may be very useful in the search of new particles and interactions in a  $e^-e^+$  Linear Collider (LC) [1] operated in the  $\gamma\gamma$  mode [2]. We find that for such an LC,  $\gamma\gamma \rightarrow \gamma\gamma$  scattering may be a very useful tool for new physics searches.

The invariant helicity amplitudes  $F_{\lambda_1\lambda_2\lambda_3\lambda_4}$  for the process

$$\gamma(p_1, \lambda_1)\gamma(p_2, \lambda_2) \rightarrow \gamma(p_3, \lambda_3)\gamma(p_4, \lambda_4) \quad , \quad (1)$$

(where the momenta and helicities of the various photons are indicated in parenthesis), satisfy  $F_{\lambda_1\lambda_2\lambda_3\lambda_4} = F_{-\lambda_1-\lambda_2-\lambda_3-\lambda_4}$  because of parity conservation, and are determined in the Standard Model (SM) by 1-loop diagrams involving contributions from charged fermions [3] and  $W^\pm$  bosons [4]. For  $\sqrt{s_{\gamma\gamma}} \gtrsim 250\text{GeV}$ , the basic features of these amplitudes are the dominance of the  $W$  contribution over the quark and leptonic ones; and the fact that only the amplitudes

$$\begin{aligned} F_{\pm\pm\pm\pm}(\hat{s}, \hat{t}, \hat{u}) \quad , \\ F_{\pm\mp\mp\pm}(\hat{s}, \hat{u}, \hat{t}) = F_{\pm\mp\pm\mp}(\hat{s}, \hat{t}, \hat{u}) \quad , \end{aligned} \quad (2)$$

are appreciable, where  $\hat{s} = (p_1 + p_2)^2$ ,  $\hat{t} = (p_3 - p_1)^2$ ,  $\hat{u} = (p_4 - p_1)^2$ , (compare 1).

The additional remarkable fact is that these dominant amplitudes are almost purely imaginary at such energies, for all scattering angles, small<sup>1</sup> [4] and large [5]. This is illustrated in Fig.1a,b [5]. Using this and the expressions in [3, 4, 5], we find that the dominant amplitudes for  $\hat{s}, |\hat{t}|, |\hat{u}| \gg M_W^2$ , are

$$F_{\pm\pm\pm\pm}(\hat{s}, \hat{t}, \hat{u}) \simeq -i 16\pi\alpha^2 \left[ \frac{\hat{s}}{\hat{u}} \text{Ln} \left| \frac{\hat{u}}{M_W^2} \right| + \frac{\hat{s}}{\hat{t}} \text{Ln} \left| \frac{\hat{t}}{M_W^2} \right| \right] \quad , \quad (3)$$

$$\begin{aligned} F_{\pm\mp\mp\mp}(\hat{s}, \hat{t}, \hat{u}) \simeq & -i 12\pi\alpha^2 \frac{s-t}{u} + \frac{8\pi\alpha^2}{\hat{u}^2} (4\hat{u}^2 - 3\hat{s}\hat{t}) \left[ \text{Ln} \left| \frac{\hat{t}}{\hat{s}} \right| \right] \\ & -i 16\pi\alpha^2 \left[ \frac{\hat{u}}{\hat{s}} \text{Ln} \left| \frac{\hat{u}}{M_W^2} \right| + \frac{\hat{u}^2}{\hat{s}\hat{t}} \text{Ln} \left| \frac{\hat{t}}{M_W^2} \right| \right] \quad , \end{aligned} \quad (4)$$

which imply that at  $\vartheta^* = 90^\circ$   $F_{\pm\pm\pm\pm} \simeq 4F_{\pm\mp\mp\mp} \simeq 4F_{\pm\mp\mp\pm}$  [5]. The same expressions (2-4) imply that at small angles  $F_{\pm\pm\pm\pm} \simeq F_{\pm\mp\mp\mp}$ , while  $F_{\pm\mp\mp\pm}$  is negligible [4]; as it is also confirmed by the results of the exact computation shown in Fig.1b.

We now propose to use these properties for searching for new physics phenomena (NP), through precision measurements of the  $\gamma\gamma \rightarrow \gamma\gamma$  cross section. An NP amplitude (too weak to show up through its modulus squared) will contribute through its interference with the SM amplitude. Because of the dominance of the imaginary parts in the SM amplitudes, the only significant interference terms will pick up the imaginary part of the new amplitude. This is particularly appealing, as it allows to observe new physics effects

---

<sup>1</sup>In effect, the amplitude in (1) has the  $s$ -channel helicity conservation properties anticipated long ago on the basis of Vector Meson Dominance and Pomeron exchange. But of course the role of the Pomeron is now taken by the  $W$ -loop, which is not connected with the Pomeron in an obvious way.

characterized by amplitudes with a large imaginary part; like e.g. threshold effects due to the virtual production of pairs of new particles; resonant contributions due to the formation of neutral states coupled to  $\gamma\gamma$ ; and unitarity saturating amplitudes due to a strongly interacting scalar sector.

Before developing these, let us say a few words about the experimental aspects of the  $\gamma\gamma$  collision process, which may be studied at an  $e^+e^-$  linear collider (LC) through the laser backscattering method [1, 2]. This method should lead to  $\gamma\gamma$  collisions at energies  $E_{cm}^{\gamma\gamma} \lesssim 0.8 E_{cm}^{ee}$  with a luminosity close or even larger than the  $e^+e^-$  one  $\mathcal{L}_{ee}$ , depending on the tuning of the backscattering process. The presently contemplated value for the LC project [1] is  $\mathcal{L}_{ee} \simeq 500 - 1000 fb^{-1}$  per one or two years of running in *e.g.* the high luminosity TESLA mode at energies of  $350 - 800 GeV$ . Since the  $\gamma\gamma$  cross section is  $\bar{\sigma}(\gamma\gamma \rightarrow \gamma\gamma) \simeq 10 fb$ , for a broad range of  $\hat{s} \equiv s_{\gamma\gamma}$  at large c.m. angles ( $30^\circ < \vartheta^* < 150^\circ$ ) [4, 5], it should be possible to collect several thousands of  $\gamma\gamma \rightarrow \gamma\gamma$  events in this large energy and angle range. In this domain the measurements should be very clean and the background negligible.

Returning now to the use of  $\gamma\gamma \rightarrow \gamma\gamma$  for NP searching, we first discuss the unpolarized case, for which the cross section reads

$$\begin{aligned} \frac{d\bar{\sigma}_0}{d\cos\vartheta^*} &= \left( \frac{1}{128\pi\hat{s}} \right) \sum_{\lambda_3\lambda_4} [|F_{++\lambda_3\lambda_4}|^2 + |F_{+-\lambda_3\lambda_4}|^2] \\ &\simeq \left( \frac{1}{128\pi\hat{s}} \right) [(ImF_{++++})^2 + (ImF_{+--+})^2 + (ImF_{+--+})^2] . \end{aligned} \quad (5)$$

Writing  $F = F^{SM} + F^{new}$ , the dominant contribution containing the new amplitude will be

$$\begin{aligned} \frac{d\bar{\sigma}_0}{d\cos\vartheta^*} &\simeq \left( \frac{1}{64\pi\hat{s}} \right) [ImF_{++++}^{SM} ImF_{++++}^{new} \\ &\quad + ImF_{+--+}^{SM} ImF_{+--+}^{new} + ImF_{+--+}^{SM} ImF_{+--+}^{new}] . \end{aligned} \quad (6)$$

As a first illustration we consider the contribution to  $\gamma\gamma \rightarrow \gamma\gamma$  from a box loop in which a new charged particle  $X^\pm$  circulates.  $X^\pm$  may be a fermion, (like *e.g.* a chargino), or a charged scalar (like a charged Higgs, a sfermion or a technipion). The imaginary part of the new amplitudes can be obtained from the expressions given in [3, 4] and reproduced in [5], in terms of the 1-loop  $B, C, D$  functions, using the imaginary parts

$$ImB(\hat{s}) = \pi \sqrt{1 - \frac{4M_X^2}{\hat{s}}} \theta(\hat{s} - 4M_X^2) , \quad (7)$$

$$ImC(\hat{s}) = -\frac{2\pi}{\hat{s}} Ln \left| \sqrt{\frac{\hat{s}}{4M_X^2}} \left( 1 + \sqrt{1 - \frac{4M_X^2}{\hat{s}}} \right) \right| \theta(\hat{s} - 4M_X^2) , \quad (8)$$

$$ImD(\hat{s}, \hat{t}) = \frac{\pi}{\sqrt{\hat{s}^2 \hat{t}^2 + 4M_X^2 \hat{s} \hat{t}}} Ln \left| \frac{(x^+ - x_a)(x^- - x_b)}{(x^- - x_a)(x^+ - x_b)} \right| \theta(\hat{s} - 4M_X^2) , \quad (9)$$

with

$$x^\pm = \frac{1}{2} \left[ 1 \pm \sqrt{1 - \frac{4M_X^2}{\hat{s}}} \right] , \quad x_{a,b} = \frac{1}{2} \left[ -\frac{\hat{t}}{\hat{u}} \pm \sqrt{\frac{\hat{t}^2}{\hat{u}^2} + \frac{4M_X^2 \hat{t}}{\hat{s}\hat{u}}} \right] . \quad (10)$$

Thus for a fermion  $X^\pm$ -particle loop, we obtain

$$\begin{aligned} ImF_{++++}^f(\hat{s}, \hat{t}, \hat{u}) &= 8\alpha^2 Q_X^4 M_X^2 (s - 2M_X^2) [ImD(\hat{s}, \hat{t}) + ImD(\hat{s}, \hat{u})] , \\ ImF_{++\mp\mp}^f(\hat{s}, \hat{t}, \hat{u}) &= -16\alpha^2 Q_X^4 M_X^4 [ImD(\hat{s}, \hat{t}) + ImD(\hat{s}, \hat{u})] , \\ ImF_{\mp\mp\pm\pm}^f(\hat{s}, \hat{t}, \hat{u}) &= ImF_{\pm\mp\mp\pm}^f(\hat{s}, \hat{u}, \hat{t}) = \alpha^2 Q_X^4 \cdot \left\{ 8 \left( \frac{\hat{s} - \hat{t}}{\hat{u}} \right) ImB(s) \right. \\ &\quad - 8 \left[ \frac{\hat{t}^2 + s^2 - 4M_X^2 \hat{u}}{\hat{u}^2} \right] \hat{s} ImC(\hat{s}) + 8M_X^2 (\hat{u} - 2M_X^2) ImD(\hat{s}, \hat{u}) \\ &\quad \left. + \frac{4}{\hat{u}^2} [-4M_X^2 \hat{u} (M_X^2 \hat{u} + \hat{t}\hat{s}) + (2\hat{u}M_X^2 + \hat{t}\hat{s})(\hat{t}^2 + \hat{s}^2)] ImD(\hat{s}, \hat{t}) \right\} . \end{aligned} \quad (11)$$

Close to the threshold  $\hat{s} \sim 4M_X^2$ , and at  $\vartheta^* \sim 90^\circ$ , the dominant contributions from (11) are then

$$ImF_{++++}^f \simeq -ImF_{++\mp\mp}^f \simeq 8\pi\alpha^2 Q_X^4 \sqrt{1 - \frac{4M_X^2}{\hat{s}}} \theta(\hat{s} - 4M^2) \quad (12)$$

whereas the other terms  $ImF_{\mp\mp\pm\pm}^f$ ,  $ImF_{\pm\mp\mp\pm}^f$  are of higher order with respect to the small quantity  $\sqrt{1 - 4M_X^2/\hat{s}}$ .

The interference of these amplitudes with the imaginary parts of the SM ones induces a threshold effect, giving a clear signal for the production of the  $X^\pm$  particles. This is also confirmed by the exact computation shown in Fig.2a, in which the real and imaginary parts of all amplitudes are retained [5]. Thus, the unpolarized cross section reflects in a perfect way the threshold effect due to the behavior of the imaginary part of the new amplitudes, without any appreciable perturbation due to the real parts. Quantitatively the threshold effect decreases from about 10% to 5%, when  $M_X$  increases from 100 GeV to 250 GeV. This should be observable at  $\gamma\gamma$  collisions obtained through laser backscattering at an LC collider of  $E_{ee} = 800$  GeV. Qualitatively similar, but quantitatively considerably smaller predictions are also obtained for the box contribution from a scalar charged particle, [5].

On the basis of the results of Fig.2a, it is also worthy to remark that the use of  $\gamma\gamma \rightarrow \gamma\gamma$  scattering in order to search for the presence of new  $X^\pm$  particles, avoids the difficult task of studying their decay modes, in case they are actually produced. Such decay mode studies are indeed often hindered by huge backgrounds and they are also affected by (possibly many) new parameters. This is *e.g.* the case in the SUSY models, in which the new sparticle decays are affected by a large number of symmetry breaking parameters [5].

As a second illustration we consider a single neutral scalar  $X^0$  of mass  $M_X$ , which could be a neutral Higgs boson, a Technipion or any other neutral scalar state. The imaginary parts of the new (resonant) amplitudes are

$$ImF_{++++}^{X^0} = ImF_{++\mp\mp}^{X^0} = 16\pi \frac{M_X^2 \Gamma_{X \rightarrow \gamma\gamma} \Gamma_X}{(\hat{s} - M_X^2)^2 + M_X^2 \Gamma_X^2} , \quad (13)$$

which substituted in (6) create the effect shown in Fig.2b when  $M_X = 400 \text{ GeV}$ ,  $\Gamma_X = 10 \text{ GeV}$  and  $\Gamma_{X \rightarrow \gamma\gamma} = 10^{-4} \text{ GeV}$ .

Using (6), (3)-(2) and (13) we see that the observability of a  $\gtrsim 3\%$  effect in  $\bar{\sigma}_0$  around  $\hat{s} \simeq M_X^2$ , requires a branching ratio  $B(X \rightarrow \gamma\gamma) \equiv \Gamma_{X \rightarrow \gamma\gamma}/\Gamma_X \gtrsim (0.5 - 1) \times 10^{-5}$  when  $M_X$  lies in the several hundreds of GeV range. This condition is satisfied in many cases; like e.g. for a standard Higgs with  $m_H \lesssim 400 \text{ GeV}$ ; and for the MSSM Higgs particles  $H$ ,  $A$  with masses up to the TeV range [6, 7]. In the technicolour case, things are more model dependent, [8]; but usually the  $\gamma\gamma$  branching ratio for a technipion is much higher than in the Higgs case, so that one can expect an even clearer effect; see *e.g.* [9] where the enormous values of  $10^{-2}$  to  $10^{-3}$  are quoted.

As a last example we quote the case of a new amplitude due to the formation of a broad scalar or due to the unitarity saturating mechanism associated to a strongly interacting sector [10]. Such an amplitude has the tendency of being purely imaginary, as one can see from a broad Breit-Wigner expression or more generally from a diffractive picture generalizing the  $VV \rightarrow VV$  hadronic case. It would then also directly show up in  $\gamma\gamma \rightarrow \gamma\gamma$  according to eq.(6). The effect could start at the threshold by the production of the lightest pair of charged particles (like e.g charged technipions), and it may stand up to the highest available energy, through the addition of the full spectrum of states associated to this new sector. Writing as a simple ansatz

$$ImF_{\pm\pm\pm\pm}^{sat} = ImF_{\pm\pm\mp\mp}^{sat} = 16\pi B_{\gamma\gamma} \sin^2 \left( \frac{\pi}{2} \left( 1 - \frac{4M_P^2}{\hat{s}} \right)^{1/2} \right) \quad (14)$$

with  $M_P = 200 \text{ GeV}$  and  $B_{\gamma\gamma} = 10^{-4}$ , one obtains the effect depicted in Fig.2c.

Let us add a short discussion on the possible use of polarized  $\gamma\gamma$  collisions in an LC operated in the  $\gamma\gamma$  mode. With Parity invariance and Bose statistics the general form of the polarized  $\gamma\gamma$  cross section in an LC simplifies to [11], [5]

$$\begin{aligned} \frac{d\sigma}{d\tau d\cos\theta^*} &= \frac{d\mathcal{L}_{\gamma\gamma}}{d\tau} \left\{ \frac{d\bar{\sigma}_0}{d\cos\theta^*} + \langle \xi_2 \tilde{\xi}_2 \rangle \frac{d\bar{\sigma}_{22}}{d\cos\theta^*} + [\langle \xi_3 \rangle \cos 2\phi + \langle \tilde{\xi}_3 \rangle \cos 2\tilde{\phi}] \frac{d\bar{\sigma}_3}{d\cos\theta^*} \right. \\ &\quad + \langle \xi_3 \tilde{\xi}_3 \rangle \left[ \frac{d\bar{\sigma}_{33}}{d\cos\theta^*} \cos 2(\phi + \tilde{\phi}) + \frac{d\bar{\sigma}'_{33}}{d\cos\theta^*} \cos 2(\phi - \tilde{\phi}) \right] \\ &\quad \left. + [\langle \xi_2 \tilde{\xi}_3 \rangle \sin 2\tilde{\phi} - \langle \xi_3 \tilde{\xi}_2 \rangle \sin 2\phi] \frac{d\bar{\sigma}_{23}}{d\cos\theta^*} \right\} , \end{aligned} \quad (15)$$

where  $d\bar{\sigma}_0/d\cos\theta^*$  is given in (5), and

$$\frac{d\bar{\sigma}_{22}}{d\cos\theta^*} = \left( \frac{1}{128\pi\hat{s}} \right) \sum_{\lambda_3\lambda_4} [|F_{++\lambda_3\lambda_4}|^2 - |F_{+-\lambda_3\lambda_4}|^2] , \quad (16)$$

$$\frac{d\bar{\sigma}_3}{d\cos\theta^*} = \left( \frac{-1}{64\pi\hat{s}} \right) \sum_{\lambda_3\lambda_4} Re[F_{++\lambda_3\lambda_4} F_{-+\lambda_3\lambda_4}^*] , \quad (17)$$

$$\frac{d\bar{\sigma}_{33}}{d\cos\theta^*} = \left( \frac{1}{128\pi\hat{s}} \right) \sum_{\lambda_3\lambda_4} Re[F_{+-\lambda_3\lambda_4} F_{-+\lambda_3\lambda_4}^*] , \quad (18)$$

$$\frac{d\bar{\sigma}'_{33}}{d\cos\theta^*} = \left(\frac{1}{128\pi\hat{s}}\right) \sum_{\lambda_3\lambda_4} \text{Re}[F_{++\lambda_3\lambda_4} F_{--\lambda_3\lambda_4}^*] , \quad (19)$$

$$\frac{d\bar{\sigma}_{23}}{d\cos\theta^*} = \left(\frac{1}{64\pi\hat{s}}\right) \sum_{\lambda_3\lambda_4} \text{Im}[F_{++\lambda_3\lambda_4} F_{+-\lambda_3\lambda_4}^*] . \quad (20)$$

In (15) the quantity  $d\mathcal{L}_{\gamma\gamma}/d\tau$  describes the overall photon-photon luminosity (per unit  $e^-e^+$  flux) in an LC operated in the  $\gamma\gamma$  mode [2], while  $\tau \equiv s_{\gamma\gamma}/s_{ee}$ . The Stokes parameters  $\xi_2$  and  $-\xi_3 e^{-2i\phi}$  in (15), determine the normalized helicity density matrix of one of the backscattered photons  $\rho_{\lambda\lambda'}^{BN}$  through [11]

$$\xi_2 = \rho_{++}^{BN} - \rho_{--}^{BN} , \quad -\xi_3 e^{-2i\phi} = \rho_{+-}^{BN} . \quad (21)$$

Thus,  $\xi_2$  describes the average longitudinal polarization of the backscattered photon, while  $\xi_3$  determines the magnitude of the transverse linear polarization, whose direction is defined by the azimuthal angle  $\phi$ , with respect to the photon momentum. Finally  $\tilde{\xi}$  and  $\tilde{\phi}$  refer to the second photon.

By making measurements with various choices of polarizations of both of the backscattered photons (which is achieved by suitable choices of the  $e^\pm$  and laser photon polarizations), all five quantities in (16-20) can be determined. The standard (SM) contributions to these (integrated in the range  $30^\circ < \vartheta^* < 150^\circ$ ) are plotted in Fig.3. At large energy the results are exactly the ones that one expects from the amplitudes given in eq.(3-2) and Fig.1; *i.e.*

$$\frac{\bar{\sigma}_{22}}{\bar{\sigma}_0} \simeq 0.5 , \quad \frac{\bar{\sigma}_3}{\bar{\sigma}_0} \simeq 0.01 , \quad \frac{\bar{\sigma}_{33}}{\bar{\sigma}_0} \simeq 0.1 , \quad \frac{\bar{\sigma}'_{33}}{\bar{\sigma}_0} \simeq 0.02 , \quad \frac{\bar{\sigma}_{23}}{\bar{\sigma}_0} \simeq 0.01 . \quad (22)$$

When new physics amplitudes like those in eq.(11,13,14) are added, then the dominance in the SM part of the purely imaginary amplitudes listed in eq.(3-2), leads us to expect about the same type of relative effects in  $\bar{\sigma}_{22}$ ,  $\bar{\sigma}_{33}$ ,  $\bar{\sigma}_{23}$  and in  $\bar{\sigma}_0$ . However, much larger relative effects are expected for the  $\bar{\sigma}_3$  and  $\bar{\sigma}'_{33}$  cases; since there the SM contribution is depressed, while the new physics contribution is not. For the thresholds and resonance examples illustrated above and the chosen values of the parameters, one may thus expect a 50 – 100% effect in the  $\bar{\sigma}_3$  or  $\bar{\sigma}'_{33}$  cases, whereas it was 5 – 10% in the  $\bar{\sigma}_0$  one. This enhancement compensates the fact that the number of events in  $\bar{\sigma}_3$  and  $\bar{\sigma}_{33}$  is reduced by a factor 50 – 100. In addition a sign difference appears between the case of a new fermion and the case of a new scalar. This should be observable and extremely useful for the identification of the origin of an effect; *e.g.* for disentangling a fermionic threshold from a bosonic one, leading to unitarity saturation (Fig.2a and 2c). More detailed analyses will be given elsewhere, [5].

In conclusion, with these few illustrations we have shown that indeed the  $\gamma\gamma \rightarrow \gamma\gamma$  process provides a clean way to check for the presence of new particles and interactions. This is due to the unique property of this process to have the SM contribution appearing only at the 1-loop level and to be dominated by few, purely imaginary, helicity amplitudes. As a consequence, the presence of new particles or interactions occurring at the same

level (boxes of charged particles or resonant single neutrals), would immediately lead to a clear signal. This method is independent and complementary to the one of looking at the direct production of new particles and studying their decay modes. It should be especially advantageous for the search of new particles decaying through a long chain of processes, which are difficult to extract from a background. In addition the availability of polarized  $\gamma\gamma$  collisions should give informations about the nature of the particles produced.

#### Acknowledgments

We like to thank D. Papadamou and G. Tsirigoti for help in the early stages of this work.

## References

- [1] Opportunities and Requirements for Experimentation at a Very High Energy  $e^+e^-$  Collider, SLAC-329(1928); Proc. Workshops on Japan Linear Collider, KEK Reports, 90-2, 91-10 and 92-16; P.M. Zerwas, DESY 93-112, Aug. 1993; Proc. of the Workshop on  $e^+e^-$  Collisions at 500 GeV: The Physics Potential, DESY 92-123A,B,(1992), C(1993), D(1994), E(1997) ed. P. Zerwas; E. Accomando *et.al.* Phys. Rep. **C299** (1998) 299.
- [2] I.F. Ginzburg, G.L. Kotkin, V.G. Serbo and V.I. Telnov, Nucl. Instr. and Meth. **205**, (1983) 47; I.F. Ginzburg, G.L. Kotkin, V.G. Serbo, S.L. Panfil and V.I. Telnov, Nucl. Instr. and Meth. **219**,(1984) 5; J.H. Kühn, E.Mirkes and J. Steegborn, Z. f. Phys. **C57** (1993) 615.
- [3] E.W.N. Glover and J.J. van der Bij Nucl. Phys. **B321** (1989) 561.
- [4] G. Jikia and A. Tkabladze, Phys. Lett. **B323** (1994) 453.
- [5] G.J. Gounaris, P.I. Porfyriadis F.M. Renard and G. Tsirigoti, in preparation.
- [6] J.F. Gunion, H.E. Haber, G. Kane and S. Dawson, The Higgs Hunter's Guide, Adison-Wesley, Redwood City, Ca, 1990.
- [7] M. Spira, hep-ph/9705337, Fortsch. Phys. **46** (1998) 203.
- [8] K. Lane and E. Eichten, Phys. Lett. **B352** (1995) 382; Phys. Rev. **D54** (1996) 2204.
- [9] R. Casalbuoni et al., hep-ph/9809523.
- [10] M. Chanowitz and M.K. Gaillard, Nucl. Phys. **B261** (1985) 379.
- [11] G.J. Gounaris and G. Tsirigoti, Phys. Rev. **D56** (1997) 3030, Erratum-ibid **D58** (1998) 059901.



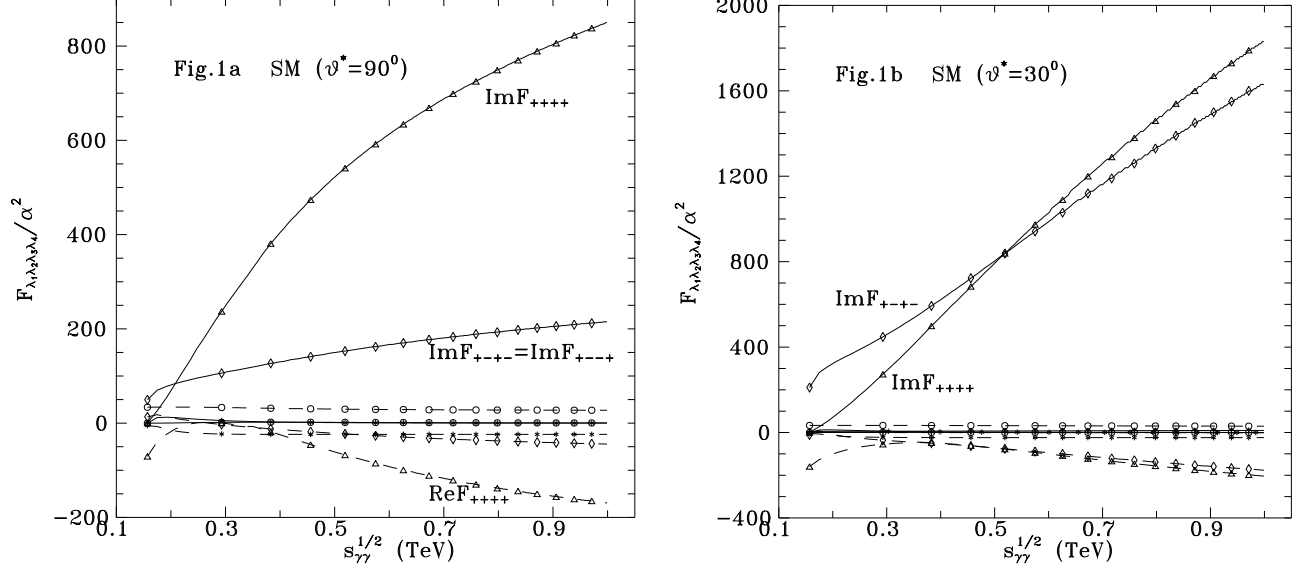


Figure 1: Imaginary (solid line) and real (dashed line) parts of the SM  $\gamma\gamma \rightarrow \gamma\gamma$  helicity amplitudes at  $\vartheta = 90^\circ$  (1a) and  $\vartheta = 30^\circ$  (1b) for  $F_{++++}$  (triangles),  $F_{+++-}$  (circles),  $F_{++--}$  (stars),  $F_{+-+-}$  (rhombs). Finally  $F_{+-+-}$  (crosses) is omitted in the (1a) case, since it is identical to  $F_{+-+-}$  at  $\vartheta = 90^\circ$ , while in the (1b) case it is negligibly small. We also note that  $F_{++++}(\hat{s}, \hat{t}, \hat{u}) = F_{+++-}(\hat{s}, \hat{t}, \hat{u}) = F_{++--}(\hat{s}, \hat{t}, \hat{u}) = F_{+-+-}(\hat{s}, \hat{t}, \hat{u})$ .

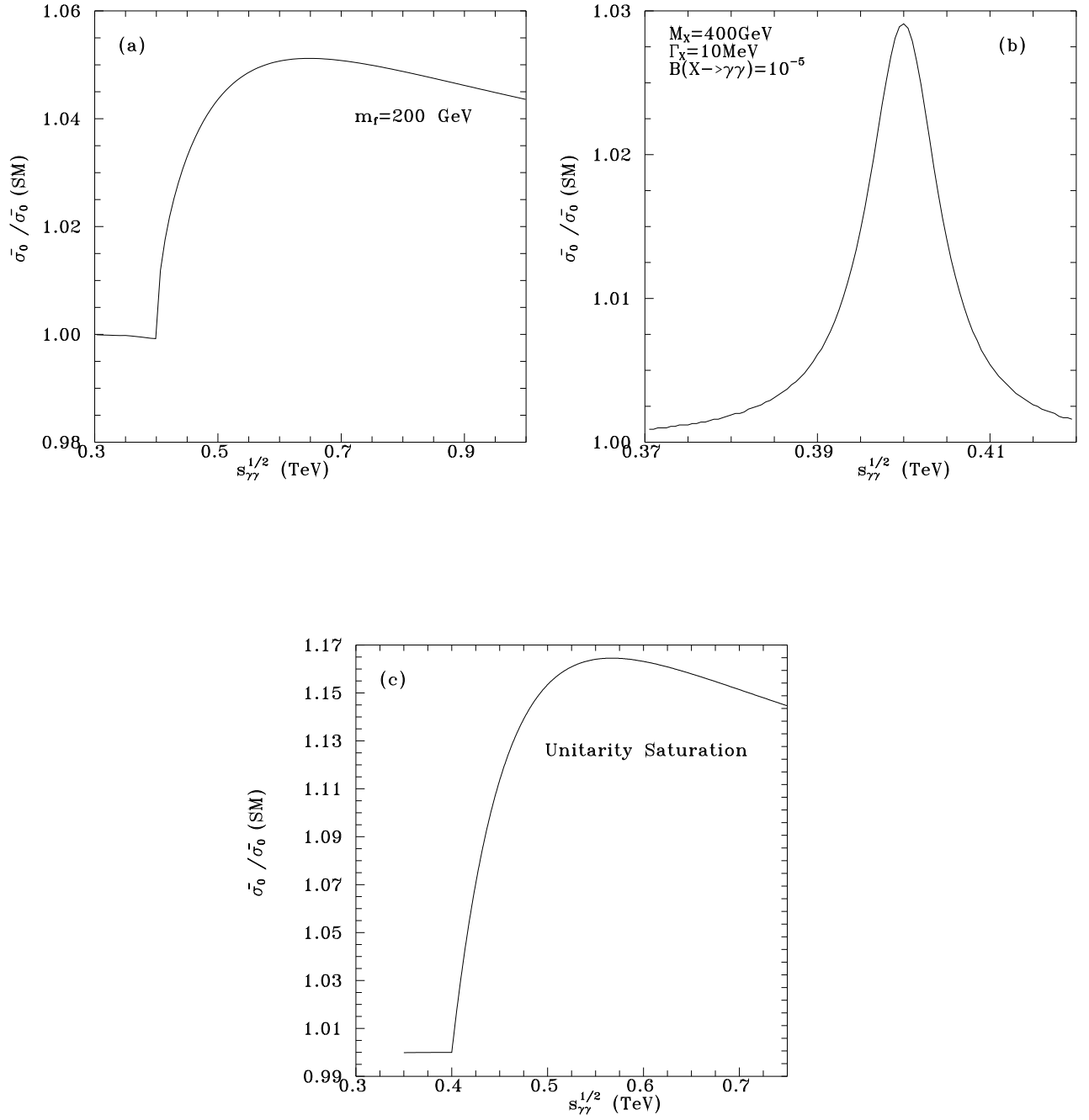


Figure 2: Relative magnitude with respect to the SM results, of the unpolarized  $\gamma\gamma \rightarrow \gamma\gamma$  cross sections for a charge +1 fermion (a), a typical s-channel neutral resonance (b), and unitarity saturating amplitudes (c). In all cases the cross sections have been integrated in the c.m. angular range  $30^\circ < \vartheta^* < 150^\circ$ .

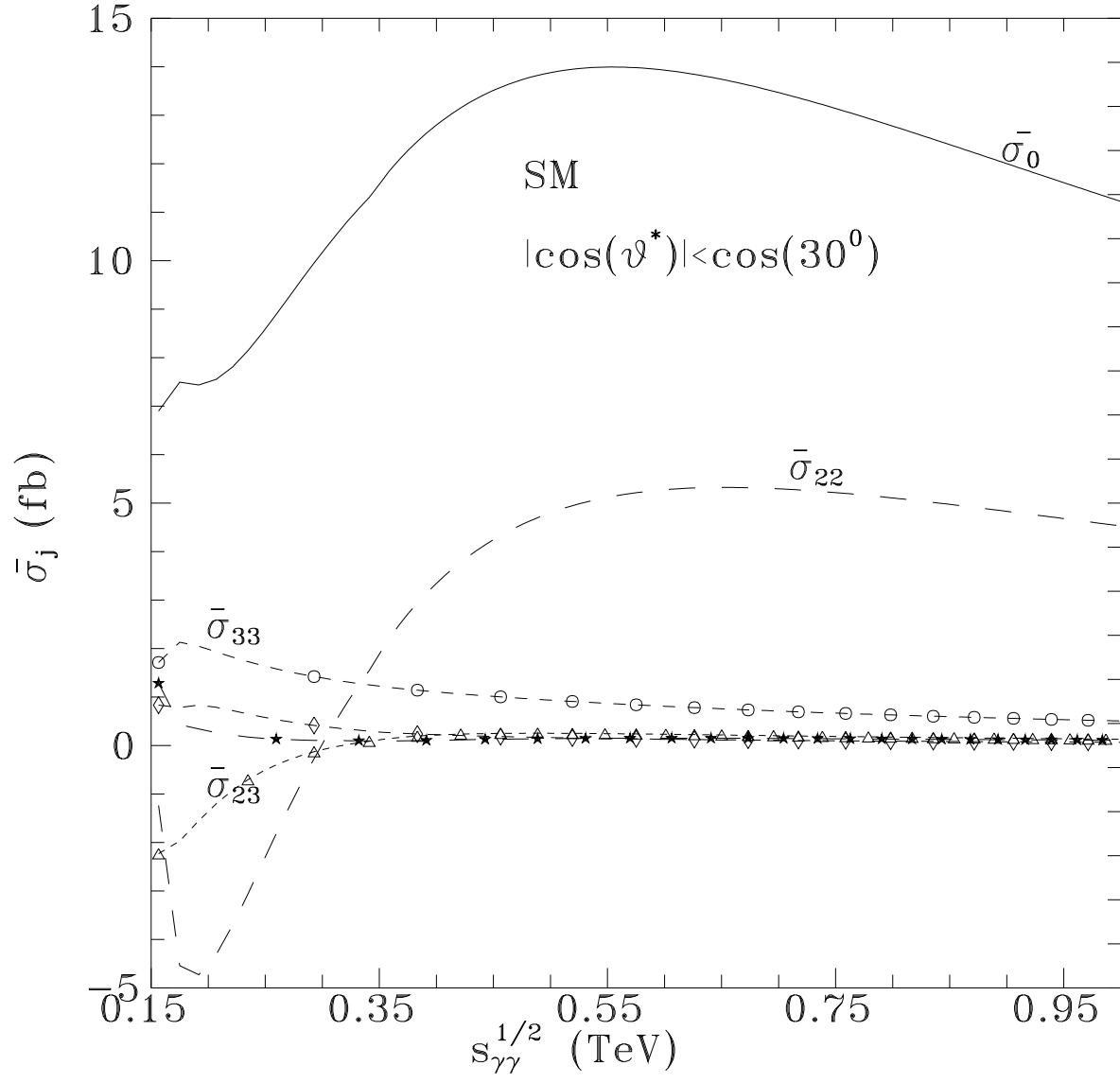


Figure 3: SM predictions for  $\bar{\sigma}_0$  (solid),  $\bar{\sigma}_{22}$  (dash),  $\bar{\sigma}_3$  (stars),  $\bar{\sigma}_{33}$  (circles),  $\bar{\sigma}'_{33}$  (rhombs),  $\bar{\sigma}_{23}$  (triangles).